EUROfusion

EUROFUSION CP(15)06/05

C. Mistrangelo et al.

Electro–Magnetic Flow Coupling for Liquid Metal Blanket Applications

12th International Symposium on Fusion Nuclear Technology (ISFNT)
Jeju Island, Korea
(14th September 2015 – 18th September 2015)

This work has been carried out within the framework of the EUROfusion Consortium and has received funding from the Euratom research and training programme 2014-2018 under grant agreement No 633053. The views and opinions expressed herein do not necessarily reflect those of the European Commission.

Electro-magnetic Flow Coupling for Liquid Metal Blanket Applications

C. Mistrangelo, L. Bühler

Karlsruhe Institute of Technology, Postfach 3640, 76021 Karlsruhe, Germany

Abstract

In the framework of the development of liquid metal blankets to be tested in ITER and for applications in a DEMOnstration reactor, magnetohydrodynamic (MHD) interactions between the electrically conducting lead lithium alloy and intense magnetic fields have been investigated numerically. In all proposed liquid metal blanket designs the presence of leakage currents that flow from one fluid domain into the adjacent one crossing electrically conducting walls has to be taken into account since it influences significantly the flow partitioning in parallel ducts. The way in which electrically coupled flows affect each other depends on orientation of common walls with respect to the magnetic field, on flow direction in adjacent channels and on the path of leakage currents. The present paper aims at providing an overview of main phenomena that occur in multiple channels where flows are coupled by an exchange of electric currents. The understanding of those basic flows is required for the study of complex 3D coupling conditions.

Key words: liquid metal blankets, magnetohydrodynamics (MHD), electrical coupling
PACS:

1. Introduction

In liquid metal blankets there are issues related to the characteristics of the liquid metal used as breeder and coolant. The interaction of the electrically conducting fluid with the magnetic field induces electric currents and electromagnetic forces that influence velocity and pressure distribution in the blanket and cause increased pressure drops compared to hydrodynamic conditions. These additional pressure losses are proportional to the electric current density induced in the fluid. The electrical conductance of the circuit formed by liquid metal and electrically conducting walls determines the magnitude of the induced currents and therefore in turn the pressure losses in the system. Therefore an analysis of the current path and its resistivity gives a good understanding of expected pressure drops. Closing of electric current paths is also affected by multi-channel effects caused by an exchange of current through electrically conducting walls that separate different fluid domains [1]. The presence of those leakage currents can lead to increased pressure drops compared to the one in separated channels and to non-uniform flow distribution in parallel ducts. In a liquid metal blanket, engineering parameters such as structural stress, local high temperature, corrosion rate and pumping power are related to the flow rates in the channels and therefore control of flow partitioning among parallel ducts is of primary importance for the thermodynamic efficiency of the system. Inhomogeneous flow distribution in multi-channel configurations is related to the non-uniformity of the electrical resistance of the current path. Flow uniformity can be enforced or enhanced by electrically coupling of parallel ducts [2]. Hua and Picologlou [3] studied MHD flows in a manifold feeding electrically coupled ducts and showed that non-uniform flow

partition can be reduced by a proper choice of wall conductances. The orientation of the magnetic field and the direction of the flow in adjacent ducts have also a significant impact on flow rates and pressure losses [4] [5]. The occurrence of these coupling phenomena is of relevance in particular for blanket concepts where no electric insulation in the ducts is foreseen, such as the helium cooled lead lithium (HCLL) blanket design.

The goal of this paper is to gain insight in the main effects of electrical coupling of MHD flows depending on orientation of the magnetic field and direction of driving pressure gradients. Moreover fully developed flows are required as inlet boundary conditions for simulations of 3D MHD flows in electrically coupled bends as studied experimentally in [6] [7]. Some preliminary 3D results in this complex configuration are shown as well.

2. Description of the problem

For the present study two geometries are considered. The first one consists of a number of square channels connected through common electrically conducting walls, as shown in Fig.1. A magnetic field is applied, which forms an angle α with the $z-$ axis. Dimensions of the channels and material properties are taken according to the ones of the experimental test section used by Stieglitz and Molokov [7] for the analysis of MHD flows in parallel electrically coupled bends.

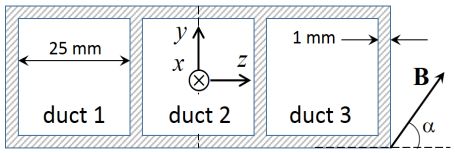

Fig. 1. Reference geometry and coordinate system for the study of electric flow coupling in parallel ducts. The middle channel is referred to as duct 2, the lateral ones as 1 and 3.

The second geometry consists of three electrically coupled rectangular bends (Fig.2). A magnetic field is applied in $y-$ direction. Dimensions of the cross-section are as shown in Fig.1 [7]. In liquid metal blankets this geometry represents a situation in which the liquid breeder flows first radially and then it turns in toroidal direction along the main component of the magnetic field. This configuration was for instance proposed for cooling of the first wall in self-cooled blanket designs [8]. A comparison of the numerical results with the experimental data allows to further validate the code in case of complex 3D flow conditions.

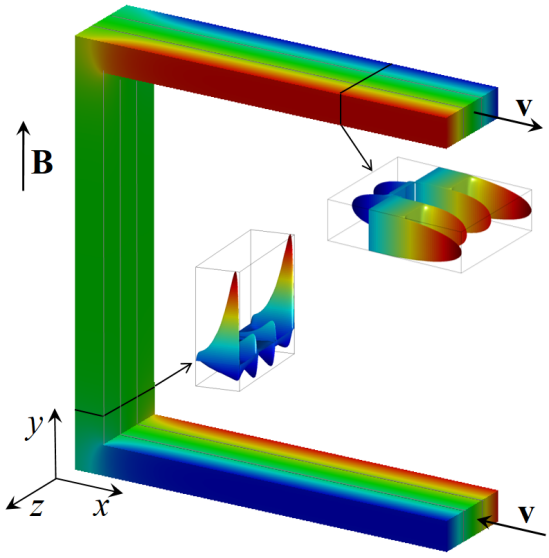

Fig. 2. Three bends with square cross section electrically coupled through common walls. Contours of electric potential on the fluid-wall interface and velocity profiles. Flow at $Ha = 1200$ and $N = 2370$.

3. Mathematical formulation

The system of non-dimensional equations describing the MHD flow of an incompressible, electrically conducting fluid includes conservation equations for momentum, mass and charge

$$\frac{1}{N}\frac{D\mathbf{v}}{Dt} = -\nabla p + \frac{1}{Ha^2}\nabla^2\mathbf{v} + \mathbf{j}\times\mathbf{B}, \qquad (1)$$

$$\nabla\cdot\mathbf{v} = 0, \qquad \nabla\cdot\mathbf{j} = 0. \qquad (2)$$

The variables $\mathbf{v}$, p, $\mathbf{j}$ and $\mathbf{B}$ indicate velocity, pressure, current density and magnetic field normalized by u_0, $\sigma u_0 B^2 L$, $\sigma u_0 B$ and B, respectively. All dimensions are scaled by half of the size of the duct, $L = 0.0125\,\mathrm{m}$, and the characteristic velocity u_0 is chosen as the average value in the cross-section of the multi-channel geometry. Fluid properties such as density ρ, electric conductivity σ and kinematic viscosity ν, are assumed to be constant. The electric current density $\mathbf{j}$ is defined by the dimensionless Ohm's law as

$$\mathbf{j} = -\nabla\phi + \mathbf{v}\times\mathbf{B}, \qquad (3)$$

where ϕ is the electric potential scaled by $u_0 BL$. The magnitude of the induced current density is determined by the resistance of the current path. In

electrically conducting ducts the wall conductance is the main parameter that controls the magnitude of currents and the ratio between conductance of the wall to the one of the fluid is expressed by the conductance parameter $c = \sigma_w t_w/(\sigma L)$. Here σ_w is the electric conductivity of the wall and t_w its thickness. The equations are written according to the so-called inductionless approximation that assumes that the magnetic field induced by currents in the fluid is negligible compared to the externally imposed one. This approximation is valid for small magnetic Reynolds numbers, $Re_m = \mu\sigma L u_0 << 1$, where μ is the magnetic permeability. The dimensionless parameters in (1) are the interaction parameter and the Hartmann number:

$$N = \frac{\sigma L B^2}{\rho u_0}, \qquad Ha = LB\sqrt{\frac{\sigma}{\rho\nu}},$$

which quantify the relative importance of electromagnetic forces to inertia and to viscous forces, respectively. The Hartmann number provides a nondimensional measure for the strength of the imposed magnetic field. At the fluid-wall interface the no-slip condition, $\mathbf{v} = 0$, is imposed and when the duct walls have finite electric conductivity wall-normal currents and electric potential are continuous

$$j_n = j_{n,w} \text{ and } \phi = \phi_w. \tag{4}$$

The analytical solution used to validate the code employes the so-called *thin wall boundary condition* [9] that is valid when the duct walls are thin ($t_w << L$). According to this approximation the wall electric potential is given by

$$\mathbf{j}\cdot\mathbf{n} = -\frac{\partial\phi}{\partial n} = \nabla\cdot(c\nabla_t\phi_w)\,, \tag{5}$$

where ∇_t denotes the components of the gradient tangential to the wall and $\mathbf{n}$ is the inward unit normal to the wall. Since the wall is thin, it is assumed that the current entering the wall turns immediately to flow only in tangential direction and therefore the potential does not vary along the wall thickness to the leading order of approximation.

4. Numerical results

Equations (1)-(3) are solved, together with a Poisson equation for the electric potential, obtained from Ohm's law (3) when electric current conservation (2) is satisfied, by using a solver developed in the finite volume open source package OpenFOAM [10]. The current density conservative scheme proposed in [11] is employed and pressure–velocity coupling is accomplished by a PISO (Pressure Implicit with Splitting of Operators) algorithm, the central difference scheme has been used for spatial discretization, while temporal discretization is first order accurate.

A typical feature of MHD flows in ducts is the formation of two types of boundary layers. Those along walls parallel to the magnetic field are called side layers and their thickness scales as $\delta_s \sim Ha^{-1/2}$, the ones at walls where the magnetic field has a normal component are the Hartmann layers and they are thinner, $\delta_{Ha} \sim Ha^{-1}$. Benchmark calculations showed that for achieving an accurate solution $7-10$ mesh points are necessary within the Hartmann layers. Higher spatial resolution in viscous boundary layers has been achieved by non-equidistant spacing.

4.1. *Benchmarking against analytical solutions*

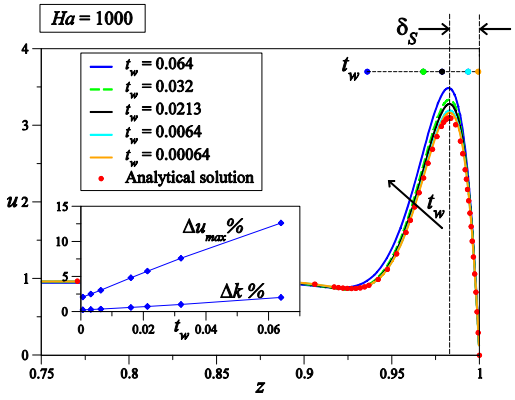

Fig. 3. Axial velocity along the transverse direction z for the MHD flow at $Ha = 1000$, $c = 0.028$ and different dimensionless thickness t_w of the duct wall. In the subplot the relative deviation of maximum velocity and of pressure gradient from the analytical solution are plotted as a function of t_w.

In order to perform simulations of 3D MHD flow in coupled bends fully developed solutions are required as inlet boundary conditions. Results for MHD flows in a single duct with $\mathbf{B} = \hat{\mathbf{y}}$ have been compared with an analytical solution to define a proper mesh. By considering dimensions of the duct according to [7] (Fig.1) a deviation of the numerical results from the analytical solution has been observed. The reason for this discrepancy is that the analytical solution employes the thin-wall boundary condition (5) to describe electrically conducting walls. The code used for the numerical simulations instead is based on the solution of coupled equations solved both in liquid metal and in walls with interface conditions

(4). A systematic study has been performed for various c and Ha and an example is shown in the following.

The influence of the finite thickness of the duct walls on the velocity distribution is shown in Fig.3 where the axial velocity is plotted along the transverse direction z for the flow at $Ha = 1000$, $c = 0.028$ and various dimensionless thicknesses t_w of the duct wall. By reducing t_w the solution approaches the analytical results valid for $t_w \to 0$. For $t_w \simeq \delta_s$ the relative error for the maximum velocity in the side layer is still $\Delta u_{\max} \simeq 5\%$ (see subplot in Fig.3). However, for all considered t_w the error for the driving pressure gradient $\nabla p = -k$ is $\Delta k < 2\%$.

4.2. *MHD flows in three electrically coupled ducts*

Numerical simulations have been performed to study MHD flows in three electrically coupled ducts (Fig.1). Various flow conditions have been investigated. Let us consider the MHD flow in ducts coupled at the side walls ($\alpha = 90°$, $\mathbf{B} = \hat{\mathbf{y}}$) for $Ha = 2500$. In the three channels the flow is driven by constant pressure gradients $k_1 = k_2 = k_3 = k$. If pressure drops in the ducts are equal, multi-channel effects result in a non-uniform flow partitioning. This type of coupling occurs in HCLL blankets for instance in the slender channels formed by cooling and horizontal stiffening plates. In Fig.4 current streamlines are plotted on the cross-section of the channel together with contours of electric potential. The current crosses the common dividing walls that behave as if they were perfectly conducting. As a result no high velocity jets are present in the side layers along the internal walls, while at the external parallel walls, where currents flow tangential to them, the velocity in the boundary layers increases significantly as expected for MHD flows in electrically conducting channels. The velocity profile along z at $y = 0$ is visualized in Fig.4. The velocity distribution is analogous to the one in a single electrically conducting duct with width $6L$; there is a uniform core and velocity jets in the side layers that form along the external walls parallel to $\mathbf{B}$. The average velocity in the outer channels is higher than in the middle one because the two side layers at the outer side walls carry a large fraction of the volume flux. These flow conditions yield a strong electric coupling of flows in neighboring ducts.

Let us consider now the case in which the ducts are coupled through the Hartmann walls ($\alpha = 0°$,

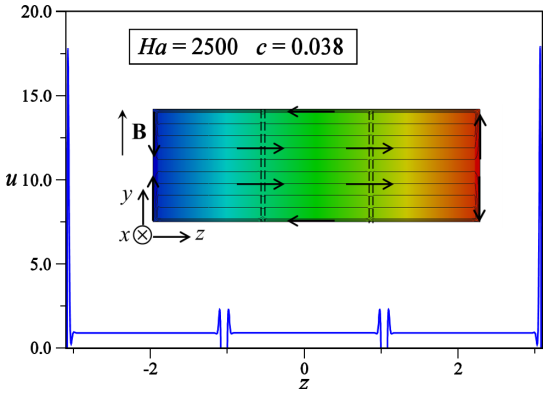

Fig. 4. Velocity profile along the central line of three ducts coupled at the side walls, $\mathbf{B} = \hat{\mathbf{y}}$, $Ha = 2500$, $c = 0.038$. The subplot shows contours of electric potential and current streamlines.

$\mathbf{B} = \hat{\mathbf{z}}$). In Fig.5 contours of electric potential and current streamlines are displayed on the duct cross-section. This type of electric coupling is similar to the one that establishes in a row of HCLL blanket breeder units that are electrically connected through the vertical stiffening plates. Practically no current is exchanged between adjacent ducts and no significant multichannel effects are observed for equal forcing pressure gradients, as shown by the velocity profiles in the middle of the ducts (Fig.5).

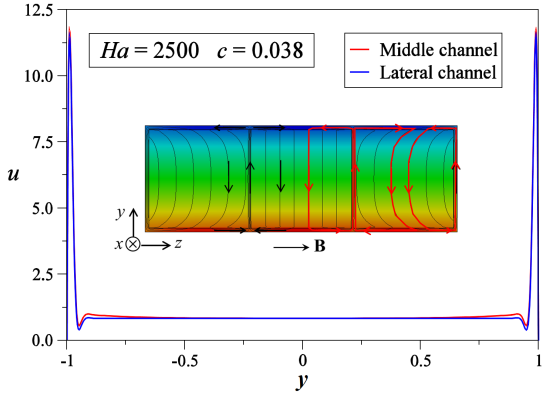

Fig. 5. Velocity profiles along y in the middle of ducts coupled at the Hartmann walls, $\mathbf{B} = \hat{\mathbf{z}}$, $Ha = 2500$, $c = 0.038$. The subplot shows contours of electric potential and current streamlines. Main current loops are marked in red in half geometry.

The crucial role of the electrical coupling in determining the velocity distribution can be clearly seen when the forcing in ducts differs. As an example we consider a case where no pressure gradient is applied in lateral channels and only the flow in the central duct is driven by a given k ($k_{1,3} = 0$, $k_2 = k$). This case is studied for $\alpha = 90°$, i.e. $\mathbf{B} = \hat{\mathbf{y}}$. The velocity

profile along z at $y = 0$ is shown in Fig.6 by a blue curve. The core velocity in the lateral ducts remains zero, while high velocity jets are observed in the side layers along the common internal parallel walls. In the lateral ducts the electric potential varies only across the side layers at the internal walls.

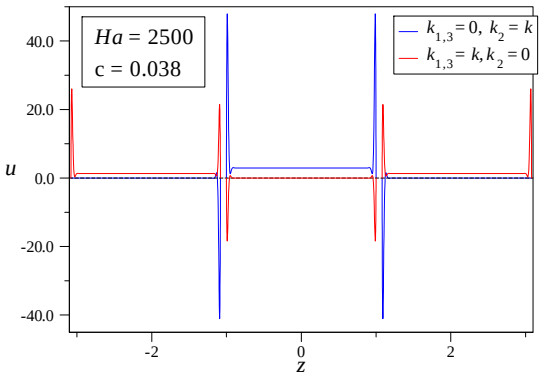

Fig. 6. Velocity profiles along the central line of three ducts coupled at the side walls, $\mathbf{B} = \hat{\mathbf{y}}$, $Ha = 2500$, $c = 0.038$. The blue curve shows the case when the flow is driven in the central duct ($k_{1,3} = 0$, $k_2 = k$); the red line the case with $k_{1,3} = k$, $k_2 = 0$.

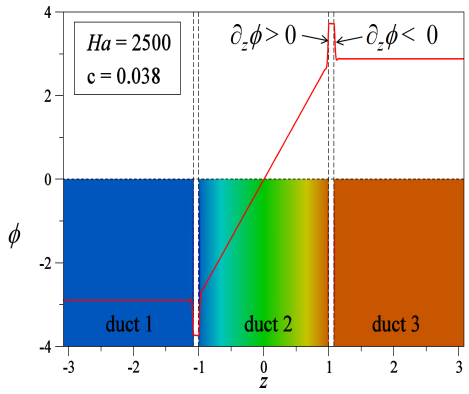

Fig. 7. Profile of electric potential along z for $\mathbf{B} = \hat{\mathbf{y}}$, $Ha = 2500$, $c = 0.038$. The flow is driven in the central duct ($k_{1,3} = 0$, $k_2 = k$). Contours of potential are also displayed.

Jets in channels 1 and 3 have opposite direction compared to the ones of the driving flow in the middle duct. This can be explained by considering the potential distribution across the side layers as visualized in Fig.7. Here the potential is plotted along the central line of the ducts at $y = 0$ and contours of potential are also displayed. The electric potential gradient across the side layers has opposite sign in the two adjacent ducts. Since according to Ohm's law (3) the electric potential gradient is proportional to the velocity ($\partial_z \phi \simeq uB$), the jets flow in opposite direction in the central and in the lateral channels. The current induced in the fluid in the core of duct 2 closes its path mainly through the side layers and the separating internal walls. A similar effect of electrical flow coupling can be observed when the flow is driven only in the lateral channels and no forcing is applied in the central one ($k_{1,3} = k$, $k_2 = 0$). The core velocity in channel 2 remains zero and high velocity jets develop in the side layers along the common parallel walls (red curve in Fig.6).

Another interesting case is the coupling of ducts across side walls, where the flow in the central duct is driven by a pressure gradient of opposite sign ($k_{1,3} = k$, $k_2 = -k$). As a result the electric current induced in the core is also reversed compared to the case with $k_{1,2,3} = k$. Current streamlines are visualized in Fig.8 with contours of electric potential. Profiles of velocity and electric potential are plotted along the central line of the ducts at $y = 0$ in Fig.9. The larger flow rate along the internal walls is due to the fact that the electric current along these walls is higher since it results from two fluid regions.

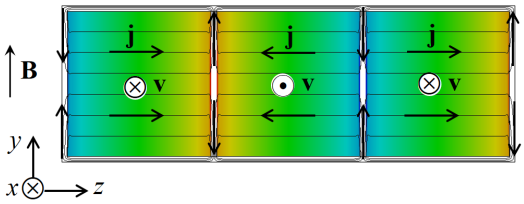

Fig. 8. Contours of electric potential and current streamlines. Ducts coupled at the side walls, $\mathbf{B} = \hat{\mathbf{y}}$, $Ha = 2500$, $c = 0.038$. The pressure gradient in the central duct has opposite sign compared to the one driving the flow in the lateral channels ($k_{1,3} = k$, $k_2 = -k$).

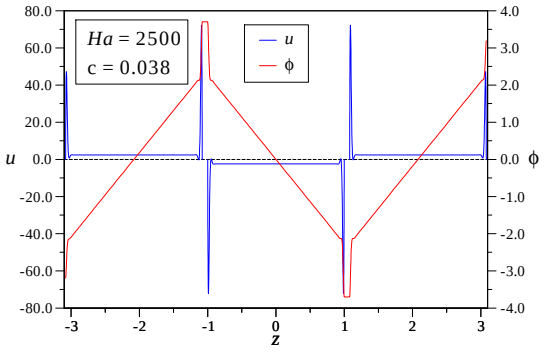

Fig. 9. Velocity and electric potential profile along the central line of three ducts coupled at the side walls ($\mathbf{B} = \hat{\mathbf{y}}$), $Ha = 2500$, $c = 0.038$. The flow in the central duct is driven by a reversed pressure gradient ($k_{1,3} = k$, $k_2 = -k$).

While the results for $k_{1,3} = k$, $k_2 = -k$ and $\mathbf{B} = \hat{\mathbf{y}}$ are not surprising, more unexpected are those obtained for $k_{1,3} = k$, $k_2 = -k$ when $\mathbf{B} = \hat{\mathbf{z}}$. Fig.10 shows for this latter case the velocity profiles along y in the middle of the three ducts. Although the flows are driven by opposite pressure gradients, the core flow in all ducts moves in the same direction. The outer ducts force the core flow in channel 2 along their own flow direction. Only in the side layers of duct 2 the flow occurs in the direction expected according to the imposed driving pressure gradient. The central duct acts as a short-circuit for the current induced in the outer channels. The major part of current closes through the cores and bypasses the common walls. This can be seen in Fig.11 where current streamlines and contours of electric potential are displayed.

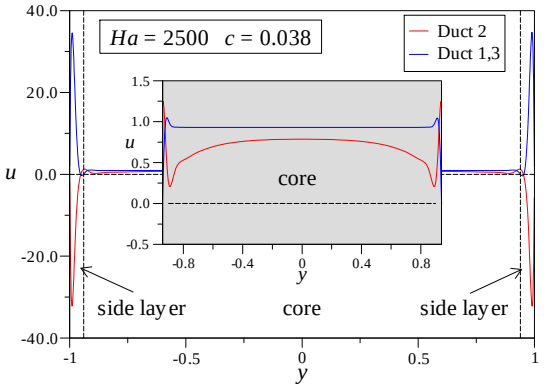

Fig. 10. Velocity profile in the ducts along $y-$ lines in the middle of the three channels, for the flow at $Ha = 2500$, $c = 0.038$ and $\mathbf{B} = \hat{\mathbf{z}}$. The velocity scale in the core region is enlarged in the subplot.

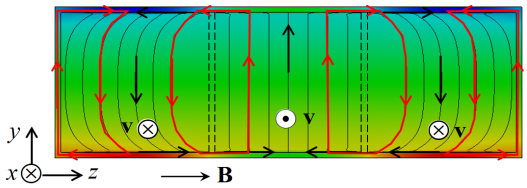

Fig. 11. Contours of electric potential and current streamlines for the flow at $Ha = 2500$, $c = 0.038$ and $\mathbf{B} = \hat{\mathbf{z}}$. Main current loops are marked in red to highlight the global current circulation.

When the magnetic field is not aligned with the walls of the duct, i.e. $0 < \alpha < 90°$, solutions for velocity and electric potential become oriented along the magnetic field lines due to the formation of internal layers that spread in the fluid from the duct corners following the magnetic field direction [12]. This yields a stronger electric coupling of the flow in the three channels due to the complex path of leakage currents. An example is shown in Fig.12 where contours of velocity magnitude and current streamlines are depicted on the cross-section of the ducts for the case of $\alpha = 45°$. The internal layers divide the fluid domains in 4 cores; 2 "internal" cores (cores 2 and 3 in Fig.12) characterized by a constant typical length along magnetic field lines, called Hartmann length, and 2 "external" cores (cores 1 and 4) where the Hartmann length reduces with the distance from the internal layers. The velocity increases significantly in the internal layers, while in cores 2 and 3 it remains relatively uniform. The latter ones are formed by the electrical coupling of two regions that belong to hydraulically separated ducts. In the external cores instead the velocity varies linearly along z. Typical current paths are shown in Fig.12. A strong electric coupling occurs and the current loops connect all the three channels. The number of cores increases if $\alpha \neq 45°$. This is displayed in Fig.13 where contours of velocity magnitude, current streamlines and the axial velocity along the central line at $y = 0$ are plotted for the case with $\alpha = 67.5°$.

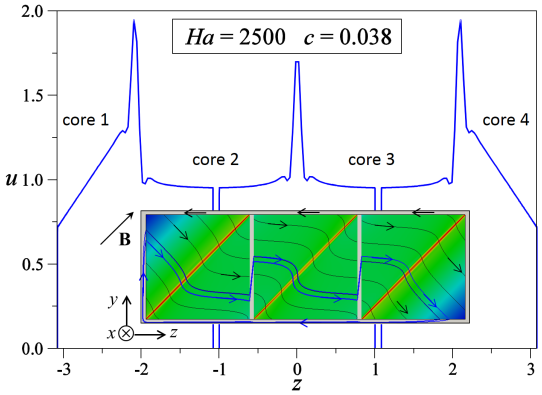

Fig. 12. Velocity profile along z in the middle of the ducts at $y = 0$ for the flow at $Ha = 2500$, $c = 0.038$ and $\alpha = 45°$. In the subplot contours of velocity magnitude and current streamlines are depicted.

5. Conclusions

Numerical simulations have been performed to study the effects of electrical coupling of adjacent fluid domains caused by leakage currents across common dividing walls. The weakest coupling occurs when ducts are coupled at the side walls and the flow is driven in opposite direction in neighboring

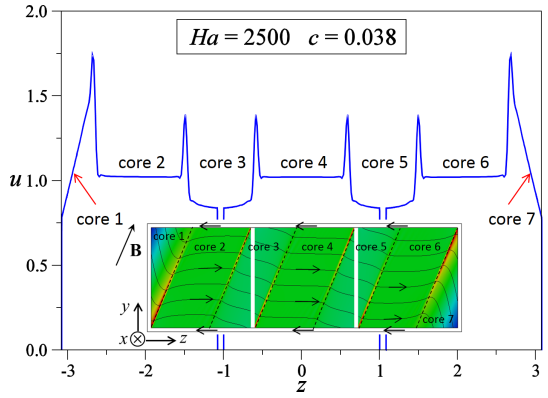

Fig. 13. Velocity profilealong z at $y = 0$ for the flow at $Ha = 2500$, $c = 0.038$ and $\alpha = 67.5°$. In the subplot contours of velocity magnitude and current streamlines are depicted.

channels. This configuration is similar to the coupling between breeder units separated by horizontal stiffening plates in a blanket column. The potential profile shown in Fig.9 resembles the one obtained experimentally in a HCLL blanket mock-up [13]. Intense multi-channel effects are present instead when ducts are connected at the side walls and the flow is driven in the same direction. In this case high velocity jets are present only at the external walls, while the flow is homogenous in the internal channels.

When ducts are coupled at Hartmann walls and the fluid is driven in the same direction by the same forcing the coupling practically does not modify the flows in the channels. This arrangement is analogous to the coupling of columns of breeder units in a HCLL blanket. A very interesting coupling occurs for counter current flows in ducts coupled at Hartmann walls. In all duct cores the fluid flows in the same direction independently of the direction of the forcing. This coupling can therefore lead to unexpected flow reversals. When the magnetic field is not aligned with the walls ($0 < \alpha < 90°$) the latter ones are all Hartmann walls, since the magnetic field always has a wall-normal component. An intense electric coupling occurs and currents circulate from one duct into the adjacent one connecting all fluid domains.

Results for fully developed flows have been applied as inlet boundary conditions for simulating 3D MHD flows in parallel bends. An example is shown in Fig.2 for the case in which the flow is driven only in the lateral ducts. Contours of electric potential are plotted on the fluid-wall interface and profiles of velocity are visualized at two different positions. At the outlet the flow is fully developed. Velocity jets appear in the side layers and in the middle duct the flow is driven by the energy supplied by the neighboring channels across the electrically conducting walls (compare red curve in Fig.6). The aim of the ongoing study is the comparison of results with experimental data to validate the code for complex 3D flow conditions.

Acknowledgment: This work has been carried out within the framework of the EUROfusion Consortium and has received funding from the Euratom research and training programme 2014-2018 under grant agreement No 633053. The views and opinions expressed herein do not necessarily reflect those of the European Commission.

References

[1] H. Madarame, K. Taghavi, M. S. Tillack, The influence of leakage currents on MHD pressure drop, Fusion Technology 8 (1985) 264–269.

[2] M. S. Tillack, N. B. Morley, Flow balancing in liquid metal blankets, Fusion Engineering and Design 27 (1995) 735–741.

[3] T. Q. Hua, B. F. Picologlou, Magnetohydrodynamic flow in a manifold and multiple rectangular coolant ducts of self-cooled blankets, Fusion Technology 19 (1991) 102–112.

[4] K. A. McCarthy, M. A. Abdou, Analysis of liquid metal MHD flow in multiple adjacent ducts using an iterative method to solve the core flow equations, Fusion Engineering and Design 13 (1991) 363–380.

[5] S. Molokov, Fully developed liquid-metal flow in multiple rectangular ducts in a strong uniform magnetic field, European Journal of Mechanics, B/Fluids 12 (6) (1993) 769–787.

[6] J. Reimann, L. Barleon, S. Molokov, I. Platnieks, E. P. A. R. Stieglitz, First results from different investigations on MHD flow in multichannel U-bends, Magnetohydrodynamics 30 (4) (1994) 448–459.

[7] R. Stieglitz, S. Molokov, Experimental study of magnetohydrodynamic flows in electrically coupled bends, Journal of Fluid Mechanics 343 (1997) 1–28.

[8] S. Malang, K. Arheidt, L. Barleon, H. U. Borgstedt, V. Casal, U. Fischer, W. Link, J. Reimann, K. Rust, G. Schmidt, Self-cooled liquid-metal blanket concept, Fusion Technology 14 (1988) 1343–1356.

[9] J. S. Walker, Magnetohydrodynamic flows in rectangular ducts with thin conducting walls, Journal de Mécanique 20 (1) (1981) 79–112.

[10] C. Mistrangelo, L. Bühler, Development of a numerical tool to simulate magnetohydrodynamic interactions of liquid metals with strong applied magnetic fields, Fusion Science and Technology 60 (2) (2011) 798–803.

[11] M.-J. Ni, R. Munipalli, N. B. Morley, P. Huang, M. A. Abdou, A current density conservative scheme for incompressible MHD flows at a low magnetic Reynolds number. Part I: On a rectangular collocated grid system, Journal of Computational Physics 227 (1) (2007) 174–204.

[12] C. J. N. Alty, Magnetohydrodynamic duct flow in a uniform transverse magnetic field of arbitrary orientation, Journal of Fluid Mechanics 48 (1971) 429–461.

[13] L. Bühler, C. Mistrangelo, Determination of flow distribution in a HCLL blanket mock-up through electric potential measurements, Fusion Engineering and Design 86 (2011) 2301–2303.